Progress in the measurement and reduction of thermal noise in optical coatings for gravitational-wave detectors

Document status and date:
Published: 01/01/2019

DOI:
10.1364/OIC.2019.FA.1

Document Version:
Publisher's PDF, also known as Version of record

Document license:
Taverne

applied optics

Progress in the measurement and reduction of thermal noise in optical coatings for gravitational-wave detectors

M. Granata,[1],* A. Amato,[1] G. Cagnoli,[2] M. Coulon,[1] J. Degallaix,[1] D. Forest,[1]
L. Mereni,[1] C. Michel,[1] L. Pinard,[1] B. Sassolas,[1] and J. Teillon[1]

[1]*Laboratoire des Matériaux Avancés–IP2I, CNRS, Université de Lyon, F-69622 Villeurbanne, France*
[2]*Université de Lyon, Université Claude Bernard Lyon 1, CNRS, Institut Lumière Matière, F-69622 Villeurbanne, France*
Corresponding author: m.granata@lma.in2p3.fr

Coating thermal noise is a fundamental limit for precision experiments based on optical and quantum transducers. In this review, after a brief overview of the techniques for coating thermal noise measurements, we present the latest worldwide research activity on low-noise coatings, with a focus on the results obtained at the Laboratoire des Matériaux Avancés. We report new updated values for the Ta_2O_5, $Ta_2O_5-TiO_2$, and SiO_2 coatings of the Advanced LIGO, Advanced Virgo, and KAGRA detectors, and new results from sputtered Nb_2O_5, $TiO_2-Nb_2O_5$, $Ta_2O_5-ZrO_2$, MgF_2, AlF_3, and silicon nitride coatings. Amorphous silicon, crystalline coatings, high-temperature deposition, multi-material coatings, and composite layers are also briefly discussed, together with the latest developments in structural analyses and models. © 2020 Optical Society of America

https://doi.org/10.1364/AO.377293

1. THE ISSUE OF COATING THERMAL NOISE

The Laboratoire des Matériaux Avancés (LMA, now a division of the newly created Institut de Physique des 2 Infinis de Lyon) has provided the current high-reflection (HR) and anti-reflective coatings of the most critical optics of Advanced LIGO [1], Advanced Virgo [2], and KAGRA [3]. In these gravitational-wave (GW) interferometers, large and massive suspended mirrors (typically with $\emptyset = 35$ cm, $t = 20$ cm, $m = 40$ kg) form the kilometer-long resonant Fabry–Perot cavities, where the astrophysical signals are embedded in the laser beam phase. Their HR coatings are Bragg reflectors of alternate layers of ion-beam-sputtered (IBS) low- and high-refractive-index materials, which feature outstanding optical properties [4]. At the same time, these amorphous coatings are the source of coating thermal noise (CTN), which is a severe limitation to the detector sensitivity [1,2].

In GW interferometers, thermal noise arises from fluctuations of the mirror surface under the random motion of particles in coatings and substrates [5,6]. Its power spectral density is determined by the amount of internal friction within the mirror materials, via the fluctuation–dissipation theorem [7]: the higher the elastic energy loss, the higher the thermal noise level. As the coating loss is usually several orders of magnitude larger than that of the substrate [8,9], CTN is the dominant source of noise in the mirrors.

More generally, CTN is a fundamental limit for precision experiments based on optical and quantum transducers, such as optomechanical resonators [10], frequency standards [11] and quantum computers [12]. In the last two decades, a considerable research effort has been committed to the measurement and the reduction of CTN.

2. MEASUREMENT

Besides kilometer-scale interferometry, several techniques are available to measure CTN. The first direct approach has been to measure the differential displacement of two suspended identical Fabry–Perot cavities in a tabletop setup [13,14]. More recently, two alternative single-cavity experiments have been successfully achieved: a single-crystal silicon Fabry–Perot cavity for cryogenic operation [15] and a folded Fabry–Perot cavity operated with higher-order laser modes [16,17]; the latter is the current reference solution for CTN measurements of the LIGO Scientific Collaboration.

An alternative option for direct CTN measurements is quadrature phase differential interferometry [18], where polarized laser beams are used in a modified Nomarski interferometer with complex contrast to measure the noise-driven displacement of a coated atomic force microscope silicon tip [19].
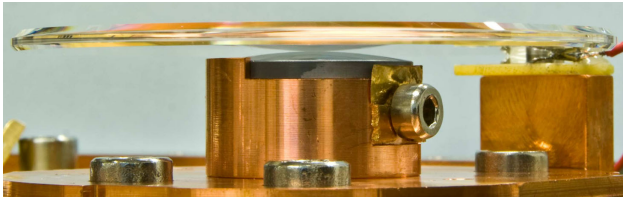
Fig. 1. Coated fused-silica disk ($\varnothing = 75$ mm) on top of a cryogenic GeNS system composed of a silicon plano–convex lens in a copper mount. An electrostatic drive, used for contactless excitation of the normal modes of the disk, is visible on the right (in the background).

An indirect approach is the measurement of the coating internal friction ϕ_c in a suspended coated resonator [20], though this measurement could be easily degraded by systematics due to the suspension system. At the LMA, we opted for a Gentle Nodal Suspension (GeNS) system [21] and adapted it for cryogenic measurements as well [22]. In such a system, shown in Fig. 1, a disk-shaped resonator of thickness t is installed on top of a spherical surface of radius r; as long as $t < 2r$ and there is no sliding between the contact surfaces, the disk is in stable equilibrium. The system can accept disks of different diameters; so far, we have tested samples ranging from 25 to 75 mm. The key features of the GeNS system are: (i) absence of clamping; (ii) extremely low excess losses ($\phi < 5 \cdot 10^{-9}$ measured for 75 mm. samples) coming from the pointlike suspension surface; (iii) unprecedented reproducibility of measurements, within a few percent on internal friction and 0.01% on resonant frequencies; and (iv) the possibility to use easily available substrates (like silicon wafers, for instance). For all these reasons, the GeNS system is now a standard setup within the Virgo and LIGO Collaborations [23,24].

With a GeNS system, measurements of internal friction are performed via the ring-down method, i.e., by measuring the ring-down time of the vibrational modes of the sample. For the i-th mode of frequency f_i and ring-down time τ_i, the measured loss is $\phi_i = (\pi f_i \tau_i)^{-1}$, and the coating loss ϕ_{c_i} can be written as

$$\phi_{c\_i} = [\phi_i + (D_i - 1)\phi_{s\_i}]/D_i , \tag{1}$$

where ϕ_{s_i} is the measured loss of the bare substrate. D_i is the so-called dilution factor, defined as the ratio of the elastic energy of the coating, E_c, to the elastic energy of the coated disk, $E = E_c + E_s$, where E_s is the elastic energy of the substrate. This ratio depends on the mode shape, and can be written as a function of the mode frequency and the mass of the sample before and after the coating deposition (f_{s_i}, f_i, m_s, and m, respectively) [19]:

$$D_i = 1 - \left(\frac{m_s}{m}\right)\left(\frac{f_{s\_i}}{f_i}\right)^2 . \tag{2}$$

Thus, thanks to the high reproducibility of frequency measurements provided by a GeNS system, the dilution factor D_i can now be measured; this implies that, unlike other experimental setups based on the ring-down method, our technique for loss characterization does not require prior knowledge of the coating Young's modulus and thickness (otherwise needed to estimate D_i). Furthermore, the coating Young's modulus (Y_c) and Poisson's ratio (ν_c) can be estimated by iteratively adjusting
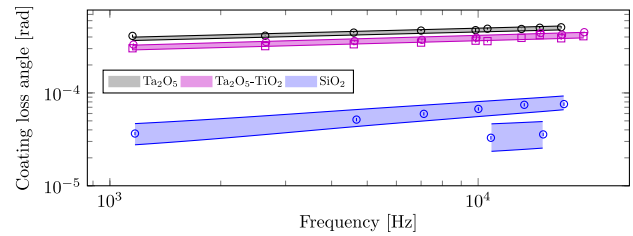
Fig. 2. Internal friction of coating materials of Advanced LIGO, Advanced Virgo, and KAGRA: Ta_2O_5, $Ta_2O_5 - TiO_2$, SiO_2. Error bars are shown, though barely visible; shaded regions represent uncertainties from fitting a frequency-dependent power-law loss model to each sample set: $\phi_c(f) = af^b$ for Ta_2O_5 and $Ta_2O_5 - TiO_2$, $\phi_c(f) = af^b + \epsilon d\phi_e$ for SiO_2, where the $\epsilon d\phi_e$ term is the spurious contribution of the coated edge of the sample [27]. The best-fit parameters of each data set are listed in Table 1.

Table 1. Mechanical Properties of Coating Layers of Advanced LIGO, Advanced Virgo, and KAGRA[a]

	a [10^{-4} rad Hz^{-b}]	b	Y_c [GPa]	ν_c
Ta_2O_5	1.88 ± 0.06	0.101 ± 0.004	117 ± 1	0.28 ± 0.01
$Ta_2O_5 - TiO_2$	1.43 ± 0.07	0.109 ± 0.005	120 ± 4	0.29 ± 0.01
SiO_2	0.20 ± 0.04	0.030 ± 0.024	70 ± 1	0.19 ± 0.01

^{a} a and b are least-squares best-fit parameters of a power-law model $\phi_c(f) = af^b$ for the measured frequency-dependent internal friction shown in Fig. 2.

finite-element simulations of coated samples to fit the measured values of D_i: the best fit is obtained with a pair (Y_c, ν_c) that minimizes the least-square figure of merit

$$m_D = \sum_i \left(\frac{D_{\text{meas}\_i} - D_{\text{sim}\_i}}{\sigma_{\text{meas}\_i}}\right)^2 , \tag{3}$$

where D_{sim_i} and ($D_{\text{meas}\_i} \pm \sigma_{\text{meas}\_i}$) are the simulated and measured dilution factors, respectively. Figure 2 compares the internal friction of coating materials of Advanced LIGO, Advanced Virgo, and KAGRA mirrors, and Table 1 summarizes their mechanical properties; all data have been measured with our GeNS system. We used a power law model $\phi_c(f) = af^b$ to describe the observed frequency-dependent behavior of the coating internal friction [25–27].
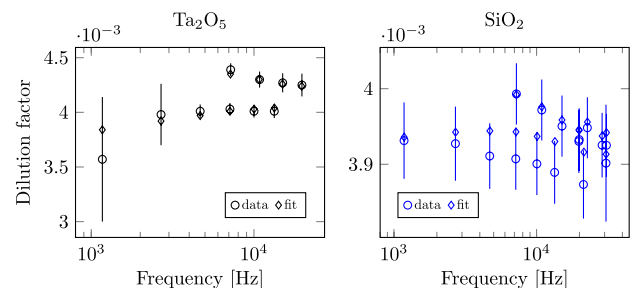
Fig. 3. Fit of measured dilution factors with simulated values for Ta_2O_5 (left) and SiO_2 (right) coatings annealed 10 h in air at 500°C. The scale of each plot is adapted to highlight the differences between measured and best-fit values.

Figure 3 shows the results of our fitting process for elastic constants of representative Ta_2O_5 and SiO_2 coating samples; the agreement between simulated and measured dilution factors vouches for the reliability of our method (though larger residuals for SiO_2 coatings seem to point out that either our model or our simulations might need further fine-tuning in some specific cases; this will be the subject of further investigation).

3. REDUCTION

In a Fabry–Perot cavity like those of GW interferometers, the frequency-dependent CTN power spectral density can be written as [9]

$$S_{CTN} \propto \frac{k_B T}{2\pi f} \frac{t_c}{w^2} \phi_c, \tag{4}$$

where f is the frequency, T is the temperature, t_c is the coating thickness, ϕ_c is the so-called coating *loss angle* that quantifies the coating internal friction, and w is the laser beam radius. Thus, besides lowering the temperature of the mirrors [3,28,29], there are three key properties that may reduce the CTN: coating thickness and internal friction, which depend on intrinsic properties of coating materials, and laser beam size, which requires the development of larger substrates and adapted deposition technology. Furthermore, the lowest coating thermal noise occurs when the coating Young's modulus is matched to that of the substrate [9]. Coating thickness is in turn a monotonically decreasing function of the refractive index contrast $c = n_H/n_L$ in the HR stack, where n_H and n_L are the high and low refractive indices, respectively; thus, the value of c, the lower the coating thickness and hence the coating thermal noise (at constant reflection).

As a consequence, the optimal coating materials would feature the lowest internal friction and the largest index contrast at the same time, a Young's modulus matching as much as possible that of the substrate to be coated (73.2 GPa in fused-silica substrates used for room-temperature operation, ≥ 130 GPa in silicon or sapphire substrates for cryogenic operation), and, in order to limit thermal lens effects, an optical absorption at least as low as it is to date, i.e., an extinction coefficient $k \sim 10^{-7}$ at $\lambda_0 = 1064$ nm (which is the wavelength of operation of GW interferometers) [4]. By taking as a reference the optical [4,30] and mechanical (Table 1) properties of the IBS oxide layers (Ta_2O_5, $Ta_2O_5-TiO_2$, SiO_2) within the HR coatings of Advanced LIGO, Advanced Virgo, and KAGRA, future low-thermal-noise coatings should have $c > 1.44$ and $\phi_c < 10^{-4}$ at 100 Hz; these and other important coating requirements are summarized in Table 2.

In order to decrease CTN, several empirical options can be considered to further optimize the coatings of current GW interferometers: tuning of the sputtering ion beam, co-sputtering (also commonly referred to as *doping*), substrate heating during deposition and post-deposition annealing. In principle, these techniques could be also combined to cumulate their benefits. Also, alternative low-friction materials may be selected, then possibly further improved.

Finally, a more fundamental approach consists of isolating and possibly inhibiting the microscopic relaxation sites [25] that determine the amount of internal friction in coatings; this

Table 2. Tentative Projection of Requirements for Optical and Mechanical Properties of Coating Layers for Future GW Interferometers, Based on Current Standards (from Refs. [4,30] and This Work)

Refractive Index	$n_H > 2.09$
	$n_L < 1.45$
Extinction	$10^{-7} < k < 10^{-6}$
Scattering	$\alpha_s \leq 10$ ppm
Internal friction	$\phi_c < 10^{-4}$ at 100 Hz
Coated diameter	$d \geq 35$ cm
Thickness uniformity	$\Delta t_c \leq 0.1\%$
Surface roughness	≤ 0.1 nm rms

approach is based on the thorough investigation of the relation between the microscopic structure of the coating materials and their macroscopic properties, both experimentally and through molecular dynamics simulations.

A. Deposition Parameters and Annealing

We studied the impact of different deposition parameters and of post-deposition annealing on the internal friction of silica (SiO_2) and tantala (Ta_2O_5) coatings, deposited with three different IBS coaters at LMA: the custom-developed so-called DIBS and Grand Coater (GC) and a commercial Veeco SPECTOR; the GC is used to coat the mirrors of GW detectors. Deposition parameters that may have a relevant impact on the coating properties are the beam ion energy and current and the geometric configuration of the elements inside the chamber, i.e., the distances and the angles between the sputtering sources, the sputtered targets, and the substrates to be coated. Each coater has its own specific set of values for these parameters, optimized to yield the highest coating optical quality, resulting in a different deposition rate. However, in all the coaters, the ion energy and current are of the order of 1 keV and 0.1 A, respectively.

Figure 4 shows the results of this preliminary study. We found no correlation between the measured loss and the distances of targets and substrates. For the Ta_2O_5 coatings, the GC provided the slowest rate and lowest loss values, whereas the SPECTOR had the fastest rate (3 Å/s) and the highest loss values. For the SiO_2 coatings, we observed that indeed the SPECTOR sample had the fastest deposition rate (2 Å/s) and the highest loss values; however, despite having the same deposition rate (within 25% experimental uncertainty), the DIBS sample had lower loss values than those of the GC sample. While this inconsistency will be the subject of further investigation, we may conclude that, as a rule of thumb, the faster the deposition rate, the higher the loss.

The post-deposition annealing decreases the internal friction: depending on the initial values considered, the reduction of internal friction is of a factor of 1.5 to 2.5 for Ta_2O_5 films, and 5 to 6.5 for SiO_2 films. As the substrates are treated at 900°C prior to deposition, the observed loss change upon annealing is due to the coating only. Once annealed, all the Ta_2O_5 films showed equal loss, as if their deposition history had been erased and an ultimate common structural configuration had been attained, whereas the gap between the loss values of SiO_2 films just decreased.
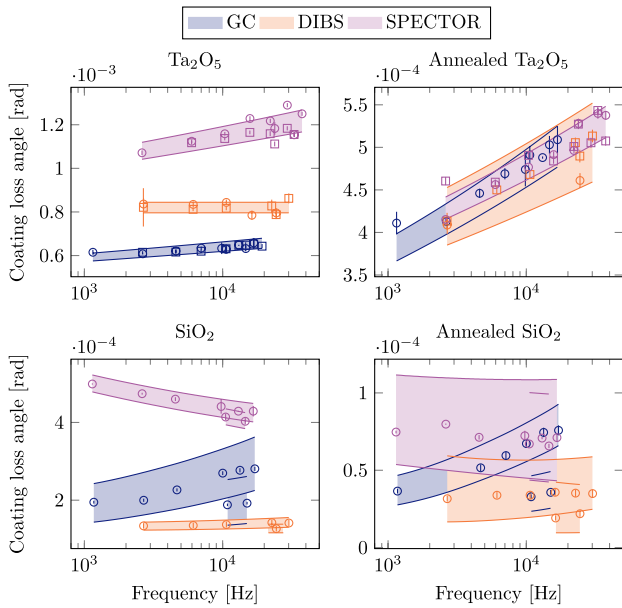
Fig. 4. Internal friction of Ta_2O_5 (top row) and SiO_2 (bottom row) coatings before (left column) and after (right column) 10 h in-air annealing at 500 °C, deposited by different coaters: GC, DIBS, and SPECTOR. Shaded regions represent uncertainties from fitting a frequency-dependent power-law loss model to each sample set: $\phi_c(f) = a f^b$ for Ta_2O_5 and $\phi_c(f) = a f^b + \epsilon d\phi_e$ for SiO_2, where the $\epsilon d\phi_e$ term is the spurious contribution of the coated edge of the sample [27]. The scale of each plot is adapted to highlight differences or similarities between different data sets.

B. Alternative Oxides and Doping

To increase the refractive index contrast by replacing the current co-sputtered $Ta_2O_5-TiO_2$ layers with higher-index materials, we tested $Ta_2O_5-TiO_2$ coatings with different Ti/Ta mixing ratios [31], Nb_2O_5 layers, and co-sputtered $TiO_2-Nb_2O_5$ coatings. Also, following preliminary results from the LIGO Collaboration, we tried $Ta_2O_5-ZrO_2$ coatings treated at higher annealing temperatures. Figure 5 shows the results of internal friction for such oxide coatings; none of them yielded significantly lower friction compared to the current $Ta_2O_5-TiO_2$ layers.

Interestingly, Fig. 5 also shows that despite their different nature and different annealing temperatures T_a, all the high-index oxide coatings characterized so far (Ta_2O_5, $Ta_2O_5-TiO_2$, Nb_2O_5, $TiO_2-Nb_2O_5$, and $Ta_2O_5-ZrO_2$) have similar internal friction values ($2 \cdot 10^{-4} \lesssim \phi_c \lesssim 5 \cdot 10^{-4}$) in the sampled frequency band, suggesting that this might be a general feature of this kind of coating. Also, the measured values are in agreement with the behavior reported in the literature for many amorphous solids [32].

C. Fluorides

To increase the refractive index contrast by replacing SiO_2 layers with lower-index materials, we characterized the optical properties and the internal friction of IBS MgF_2 and AlF_3 coatings produced by the Laser Zentrum Hannover. Before annealing, we measured a lower refractive index ($n_{MgF2} = 1.40$, $n_{AlF3} = 1.36$ at 1064 nm) but observed a too-large optical
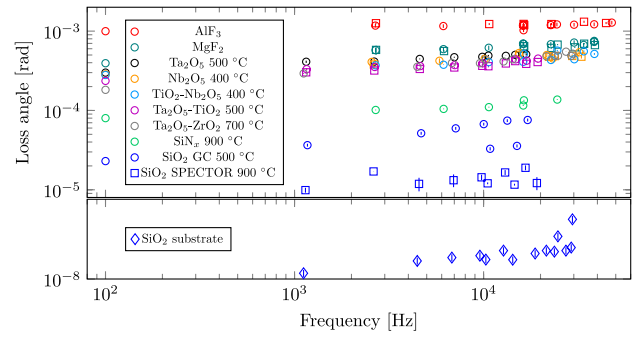
Fig. 5. Internal friction of IBS coatings (for annealed samples, the in-air annealing temperature T_a is indicated in the legend and annealing time is 10 h), compared to that of a representative substrate; values at 100 Hz are extrapolations from fitting a power-law loss model to each sample set.
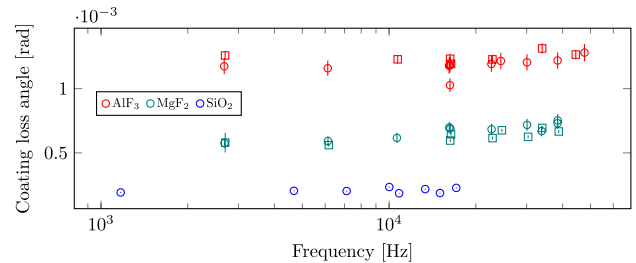
Fig. 6. Internal friction of as-deposited IBS coatings: AlF_3 and MgF_2, compared to SiO_2 deposited in the GC.

absorption of $5 \cdot 10^{-5} < k < 10^{-4}$. Also, as Fig. 6 shows, the coatings' internal friction is much greater than that of current as-deposited SiO_2 layers. Work is ongoing to characterize the impact of annealing on their absorption and internal friction; soon we will also measure their low-temperature internal friction, for possible implementation in future interferometers [3,28,29].

D. Silicon Nitride

Because of their low internal friction [33], we also decided to test silicon nitride (SiN_x) coatings. Usually, such coatings are deposited by chemical vapor deposition (CVD), resulting in high optical absorption ($k \sim 1 - 5 \cdot 10^{-5}$) due to hydrogen contamination [34]; moreover, their thickness uniformity still remains to be tested against the stringent requirements of GW detectors. Thus we chose to develop our own IBS SiN_x coatings and test their loss versus the annealing temperature [31]. The latest results are shown in Figs. 5 and 7: after in-air annealing at 900°C for 10 h, our IBS SiN_x coatings have more than 3 times lower loss than present $Ta_2O_5-TiO_2$ coatings. However, though lower than that of CVD coatings, their absorption is still too high ($10^{-6} < k < 10^{-5}$), so we are presently working to further reduce this value.

Another remarkable advantage of silicon nitride coatings is their much higher crystallization temperature; we could anneal our IBS SiN_x layers up to 900°C without observing crystallization. Since the crystallization temperature of our SiO_2 coatings
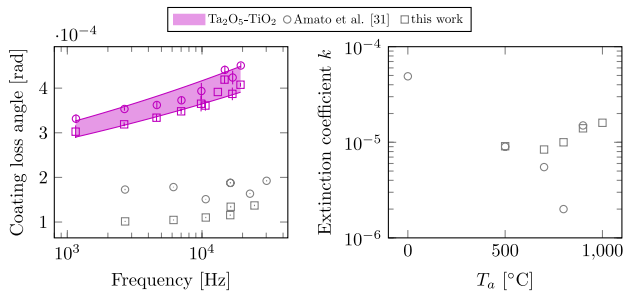
Fig. 7. Characterization of IBS SiN$_x$ coatings. Left: internal friction of our first [31] and latest coating samples annealed in air at 900°C for 10 h, compared to current values of Ta$_2$O$_5$−TiO$_2$ coatings annealed in air at 500°C for 10 h (from Fig. 2). Right: extinction coefficient of our first [31] and latest coating samples as a function of the annealing temperature T_a (in-air annealing time is 10 h, $T_a = 0$°C corresponds to as-deposited coatings).

is higher than 900°C [31], an HR stack of SiN$_x$ and SiO$_2$ could be annealed at a higher temperature, also decreasing the loss of SiO$_2$ layers [31] and thus the CTN of the whole stack.

E. Amorphous Silicon

Recent results [35–37] have shown that coatings of amorphous silicon (aSi) deposited through various techniques (e-beam evaporation, reactive low-voltage ion plating, IBS) can feature very a high refractive index ($n \sim 3.6$) and very low internal friction ($10^{-5} < \phi_c < 10^{-4}$). However, their optical absorption ($10^{-5} < k < 10^{-4}$ for $1064 < \lambda < 2000$ nm and $20 < T < 290$ K) is still too high to meet the requirements of GW interferometers.

F. Substrate Heating

Silicon nitride coatings prepared by low-pressure CVD on substrates heated at 850°C [33] and aSi coatings deposited at relatively high temperatures ($T_s = 200−400$°C) by a variety of deposition techniques [35–37] have shown that substrate heating during deposition is a promising technique for obtaining coatings with very low internal friction ($10^{-6} < \phi_c < 10^{-4}$) at room and cryogenic temperatures.

The high-temperature deposition of IBS Ta$_2$O$_5$ coatings has also been explored [38], but it seems to have a negligible impact on the room-temperature internal friction of coatings deposited at $150 < T_s < 500$°C.

At LMA, we have now completed the installation of a rotating heating substrate holder, in order to deposit uniform single layers and HR coatings up to $T_s = 800$°C. Soon we will use it to test the deposition of Ta$_2$O$_5$ coatings at temperatures just below their crystallization limit ($500 < T_s < 650$°C) [31] and of SiO$_2$ and silicon nitride coatings, whose crystallization occurs beyond 900°C [31].

G. Composite High-Index Layers

In order to replace the current Ta$_2$O$_5$−TiO$_2$ high-index layers of GW interferometers, the use of stacks of TiO$_2$ and SiO$_2$ with nanometer-thick layers has been proposed [39–41].

Though they have a lower refractive index ($n = 1.76$) [41], these nanometer-thick layered stacks can be annealed at a higher temperature ($700 < T_a < 800$°C) and have low internal friction at temperatures below 100 K [41]. However, to date, the deposition of a full HR stack embedding composite layers has yet to be achieved.

H. Multi-Material HR Stacks

In order to conjugate low internal friction and low optical absorption, HR stacks composed of at least three different coating materials have been proposed [42,43]. In this multi-material design (as, for instance, in Ta$_2$O$_5$/SiO$_2$/aSi [42], Ta$_2$O$_5$−TiO$_2$/SiO$_2$/SiN$_x$ [44], and Ta$_2$O$_5$/SiO$_2$/HfO$_2$−SiO$_2$/aSi [45] stacks), the low-friction absorptive layers are buried under the low-absorption dissipative layers.

Multi-material HR stacks might be a viable solution to substantially decrease CTN and, at the same time, to fulfill the optical requirements of future GW detectors (cryogenic ones in particular [44,45]). However, to date, an experimental demonstration of such systems has yet to be achieved.

I. Crystalline Coatings

Mono-crystalline semiconductors grown by molecular-beam epitaxy, like GaAs/AlGaAs [46] and GaP/AlGaP [47] coatings, feature low internal friction ($\phi_c \leq 10^{-4}$) at ambient and cryogenic temperatures. Furthermore, GaAs/AlGaAs coatings have competitive optical properties [48] when compared with current state-of-the-art IBS coatings [4]. However, the implementation of GaAs/AlGaAs coatings in high-finesse cavities presents issues yet to be solved: (i) the fact that they are not available in the large diameter ($d \geq 35$cm) required by GW interferometers, as their size is limited to date by the available size of the lattice-matched GaAs wafers required for seeded growth; (ii) the presence of a number of imperfections [49], including point defects > 50 μm in diameter and un-bonded regions (due to the transfer of the mono-crystalline stack from the growth wafer to the target optical surface); (iii) the inconsistency between the latest measured values [49] and previous estimations [46] of coating internal friction.

The GaP/AlGaP coatings have been specifically designed to overcome the current size limitation of GaAs/AlGaAs-based systems. However, due to the limited index contrast between GaP and AlGaP layers, the number of layers N required by a GaP/AlGaP design to achieve the same optical reflectivity as current GW detectors' HR coatings is large, $N > 100$ [50]; to date, N is limited to considerably lower values [50], resulting in a limited reflectivity.

J. Structural Analyses and Models

In the commonly accepted phenomenological two-level systems (TLS) model [25], for temperatures of more than several Kelvin, internal friction arises from thermally activated transitions of particle structures between equilibrium configurations within the potential energy landscape of an amorphous solid. Indeed, the TLS model still does not include several crucial details of the energy loss, such as the identification of the structure relaxing

from one equilibrium position to another and the factors that determine a particular energy distribution of TLS. As a result, a considerable amount of theoretical work is presently ongoing in order to overcome the TLS model.

As a matter of fact, the utmost scientific and technological challenge of CTN reduction may lie in the ability to isolate the relaxation sites, whose nature has remained elusive to date. By understanding which properties of amorphous structures are able to affect either the rate or the number of such transitions, it could be possible to inhibit relaxation and hence internal friction.

In recent years, the search for a structural origin of internal friction in amorphous materials has produced several sound results, from experimental correlations between dissipation and structural organization [51–53] to molecular dynamics simulations [54–57].

4. CONCLUSIONS

Coatings of precision optical and quantum transducers are required to simultaneously feature outstanding optical and mechanical properties: low internal friction for low thermal noise, as well as low optical absorption and scattering for low optical loss (also, for kilometer-scale interferometric GW detection, extreme surface figure requirements). These specifications are extraordinarily difficult to meet in a single coating material and deposition technique; to date, some promising options are IBS SiN_x and SiO_2 [31] and amorphous silicon [35–37], to be deposited [33,35] and possibly further annealed [31,33] at a high temperature. Such materials, if used in a multi-material design [42,43], might be a viable solution for the next sensitivity upgrades of Advanced LIGO and Advanced Virgo (2022-2023) and KAGRA.

In the meantime, structural analyses [51–53] and molecular dynamics simulations [54–57] might provide critical information toward a more radical solution to the coating thermal noise issue, to benefit future GW interferometers [28,29].

Disclosures.   The authors declare that there are no conflicts of interest related to this paper.

REFERENCES

1. The LIGO Scientific Collaboration, "Advanced LIGO," Class. Quantum Grav. **32**, 074001 (2015).
2. The Virgo Collaboration, "Advanced Virgo: a second-generation interferometric gravitational wave detector," Class. Quantum Grav. **32**, 024001 (2015).
3. The KAGRA Collaboration, "Interferometer design of the KAGRA gravitational wave detector," Phys. Rev. D **88**, 043007 (2013).
4. L. Pinard, C. Michel, B. Sassolas, L. Balzarini, J. Degallaix, V. Dolique, R. Flaminio, D. Forest, M. Granata, B. Lagrange, N. Straniero, J. Teillon, and G. Cagnoli, "Mirrors used in the LIGO interferometers for first detection of gravitational waves," Appl. Opt. **56**, C11–C15 (2017).
5. P. R. Saulson, "Thermal noise in mechanical experiments," Phys. Rev. D **42**, 2437–2445 (1990).
6. Y. Levin, "Internal thermal noise in the LIGO test masses: a direct approach," Phys. Rev. D **57**, 659–663 (1998).
7. H. B. Callen and R. F. Greene, "On a theorem of irreversible thermodynamics," Phys. Rev. **86**, 702–710 (1952).
8. D. R. M. Crooks, P. Sneddon, G. Cagnoli, J. Hough, S. Rowan, M. M. Fejer, E. Gustafson, R. Route, N. Nakagawa, D. Coyne, G. M. Harry, and A. M. Gretarsson, "Excess mechanical loss associated with dielectric mirror coatings on test masses in interferometric gravitational wave detectors," Class. Quantum Grav. **19**, 883–896 (2002).
9. G. M. Harry, A. M. Gretarsson, P. R. Saulson, S. E. Kittelberger, S. D. Penn, W. J. Startin, S. Rowan, M. M. Fejer, D. R. M. Crooks, and G. Cagnoli, "Thermal noise in interferometric gravitational wave detectors due to dielectric optical coatings," Class. Quantum Grav. **19**, 897–918 (2002).
10. M. Aspelmeyer, T. J. Kippenberg, and F. Marquardt, "Cavity optomechanics," Rev. Mod. Phys. **86**, 1391–1452 (2014).
11. D. G. Matei, T. Legero, S. Häfner, C. Grebing, R. Weyrich, W. Zhang, L. Sonderhouse, J. M. Robinson, J. Ye, F. Riehle, and U. Sterr, " Lasers with sub-10 mHz linewidth," Phys. Rev. Lett. **118**, 263202 (2017).
12. J. M. Martinis, K. B. Cooper, R. McDermott, M. Steffen, M. Ansmann, K. D. Osborn, K. Cicak, S. Oh, D. P. Pappas, R. W. Simmonds, and C. C. Yu, "Decoherence in Josephson qubits from dielectric loss," Phys. Rev. Lett. **95**, 210503 (2005).
13. K. Numata, M. Ando, K. Yamamoto, S. Otsuka, and K. Tsubono, "Wide-band direct measurement of thermal fluctuations in an interferometer," Phys. Rev. Lett. **91**, 260602 (2003).
14. E. D. Black, A. Villar, K. Barbary, A. Bushmaker, J. Heefner, S. Kawamura, F. Kawazoe, L. Matone, S. Meidt, S. R. Rao, K. Schulz, M. Zhang, and K. G. Libbrecht, "Direct observation of broadband coating thermal noise in a suspended interferometer," Phys. Lett. A **328**, 1–5 (2004).
15. T. Kessler, C. Hagemann, C. Grebing, T. Legero, U. Sterr, F. Riehle, M. J. Martin, L. Chen, and J. Ye, "A sub-40-mHz-linewidth laser based on a silicon single-crystal optical cavity," Nat. Photonics **6**, 687–692 (2012).
16. S. Gras, H. Yu, W. Yam, D. Martynov, and M. Evans, "Audio-band coating thermal noise measurement for Advanced LIGO with a multimode optical resonator," Phys. Rev. D **95**, 022001 (2017).
17. S. Gras and M. Evans, "Direct measurement of coating thermal noise in optical resonators," Phys. Rev. D **98**, 122001 (2018).
18. L. Bellon, S. Ciliberto, H. Boubaker, and L. Guyon, "Differential interferometry with a complex contrast," Opt. Commun. **207**, 49–56 (2002).
19. T. Li, F. A. A. Sandoval, M. Geitner, L. Bellon, G. Cagnoli, J. Degallaix, V. Dolique, R. Flaminio, D. Forest, M. Granata, C. Michel, N. Morgado, and L. Pinard, "Measurements of mechanical thermal noise and energy dissipation in optical dielectric coatings," Phys. Rev. D **89**, 092004 (2014).
20. B. S. Berry and W. C. Pritchet, "Vibrating reed internal friction apparatus for films and foils," IBM J. Res. Dev. **19**, 334–343 (1975).
21. E. Cesarini, M. Lorenzini, E. Campagna, F. Martelli, F. Piergiovanni, F. Vetrano, G. Losurdo, and G. Cagnoli, "A gentle nodal suspension for measurements of the acoustic attenuation in materials," Rev. Sci. Instrum. **80**, 053904 (2009).
22. M. Granata, L. Balzarini, J. Degallaix, V. Dolique, R. Flaminio, D. Forest, D. Hofman, C. Michel, R. Pedurand, L. Pinard, B. Sassolas, N. Straniero, J. Teillon, and G. Cagnoli, "Internal friction and Young's modulus measurements on and films done with an ultra-high Q silicon-wafer suspension," Arch. Metall. Mater. **60**, 365–370 (2015).
23. M. Granata, E. Saracco, N. Morgado, A. Cajgfinger, G. Cagnoli, J. Degallaix, V. Dolique, D. Forest, J. Franc, C. Michel, L. Pinard, and R. Flaminio, "Mechanical loss in state-of-the-art amorphous optical coatings," Phys. Rev. D **93**, 012007 (2016).
24. G. Vajente, A. Ananyeva, G. Billingsley, E. Gustafson, A. Heptonstall, E. Sanchez, and C. Torrie, "A high throughput instrument to measure mechanical losses in thin film coatings," Rev. Sci. Instrum. **88**, 073901 (2017).
25. K. S. Gilroy and W. A. Phillips, "An asymmetric double-well potential model for structural relaxation processes in amorphous materials," Philos. Mag. B **43**, 735–746 (1981).

26. F. Travasso, P. Amico, L. Bosi, F. Cottone, A. Dari, L. Gammaitoni, H. Vocca, and F. Marchesoni, "Low-frequency internal friction in silica glass," Europhys. Lett. **80**, 50008 (2007).

27. G. Cagnoli, M. Lorenzini, E. Cesarini, F. Piergiovanni, M. Granata, D. Heinert, F. Martelli, R. Nawrodt, A. Amato, Q. Cassar, J. Dickmann, S. Kroker, D. Lumaca, C. Malhaire, and C. B. R. Hurtado, "Mode-dependent mechanical losses in disc resonators," Phys. Lett. A **382**, 2165–2173 (2018).

28. The Einstein Telescope Science Team, "Sensitivity studies for third-generation gravitational wave observatories," Class. Quantum Grav. **28**, 094013 (2011).

29. The LIGO Scientific Collaboration, and J. Harms, "Exploring the sensitivity of next generation gravitational wave detectors," Class. Quantum Grav. **34**, 044001 (2017).

30. A. Amato, S. Terreni, V. Dolique, D. Forest, G. Gemme, M. Granata, L. Mereni, C. Michel, L. Pinard, and B. Sassolas, "Optical properties of high-quality oxide coating materials used in gravitational-wave advanced detectors," J. Phys.: Mater. **2**, 035004 (2019).

31. A. Amato, G. Cagnoli, M. Canepa, E. Coillet, J. Degallaix, V. Dolique, D. Forest, M. Granata, V. Martinez, C. Michel, L. Pinard, B. Sassolas, and J. Teillon, "High-reflection coatings for gravitational-wave detectors: state of the art and future developments," J. Phys. Conf. Ser. **957**, 012006 (2018).

32. K. Topp and D. G. Cahill, "Elastic properties of several amorphous solids and disordered crystals below 100 K," Z. Phys. B **101**, 235–245 (1996).

33. X. Liu, T. H. Metcalf, Q. Wang, and D. M. Photiadis, "Elastic properties of several silicon nitride films," in *Materials Research Society Symposium Proceedings* (2007), Vol. **989**, paper 0989-A22-01.

34. H.-W. Pan, L.-C. Kuo, S.-Y. Huang, M.-Y. Wu, Y.-H. Juang, C.-W. Lee, H.-C. Chen, T. T. Wen, and S. Chao, "Silicon nitride films fabricated by a plasma-enhanced chemical vapor deposition method for coatings of the laser interferometer gravitational wave detector," Phys. Rev. D **97**, 022004 (2018).

35. X. Liu, D. R. Queen, T. H. Metcalf, J. E. Karel, and F. Hellman, "Hydrogen-free amorphous silicon with no tunneling states," Phys. Rev. Lett. **113**, 025503 (2014).

36. J. Steinlechner, I. W. Martin, A. S. Bell, J. Hough, M. Fletcher, P. G. Murray, R. Robie, S. Rowan, and R. Schnabel, "Silicon-based optical mirror coatings for ultrahigh precision metrology and sensing," Phys. Rev. Lett. **120**, 263602 (2018).

37. R. Birney, J. Steinlechner, Z. Tornasi, S. MacFoy, D. Vine, A. S. Bell, D. Gibson, J. Hough, S. Rowan, P. Sortais, S. Sproules, S. Tait, I. W. Martin, and S. Reid, "Amorphous silicon with extremely low absorption: beating thermal noise in gravitational astronomy," Phys. Rev. Lett. **121**, 191101 (2018).

38. G. Vajente, R. Birney, A. Ananyeva, S. Angelova, R. Asselin, B. Baloukas, R. Bassiri, G. Billingsley, M. M. Fejer, D. Gibson, L. J. Godbout, E. Gustafson, A. Heptonstall, J. Hough, S. MacFoy, A. Markosyan, I. W. Martin, L. Martinu, P. G. Murray, S. Penn, S. Roorda, S. Rowan, F. Schiettekatte, R. Shink, C. Torrie, D. Vine, S. Reid, and R. X. Adhikari, "Effect of elevated substrate temperature deposition on the mechanical losses in tantala thin film coatings," Class. Quantum Grav. **35**, 075001 (2018).

39. H.-W. Pan, S.-J. Wang, L.-C. Kuo, S. Chao, M. Principe, I. M. Pinto, and R. DeSalvo, "Thickness-dependent crystallization on thermal anneal for titania/silica nm-layer composites deposited by ion beam sputter method," Opt. Express **22**, 29847–29854 (2014).

40. M. Magnozzi, S. Terreni, L. Anghinolfi, S. Uttiya, M. M. Carnasciali, G. Gemme, M. Neri, M. Principe, I. Pinto, L.-C. Kuo, S. Chao, and M. Canepa, "Optical properties of amorphous SiO_2-TiO_2 multi-nanolayered coatings for 1064-nm mirror technology," Opt. Mater. **75**, 94–101 (2018).

41. L.-C. Kuo, H.-W. Pan, C.-L. Chang, and S. Chao, "Low cryogenic mechanical loss composite silica thin film for low thermal noise dielectric mirror coatings," Opt. Lett. **44**, 247–250 (2019).

42. J. Steinlechner, I. W. Martin, J. Hough, C. Krüger, S. Rowan, and R. Schnabel, "Thermal noise reduction and absorption optimization via multimaterial coatings," Phys. Rev. D **91**, 042001 (2015).

43. W. Yam, S. Gras, and M. Evans, "Multimaterial coatings with reduced thermal noise," Phys. Rev. D **91**, 042002 (2015).

44. H.-W. Pan, L.-C. Kuo, L.-A. Chang, S. Chao, I. W. Martin, J. Steinlechner, and M. Fletcher, "Silicon nitride and silica quarter-wave stacks for low-thermal-noise mirror coatings," Phys. Rev. D **98**, 102001 (2018).

45. K. Craig, J. Steinlechner, P. G. Murray, A. S. Bell, R. Birney, K. Haughian, J. Hough, I. MacLaren, S. Penn, S. Reid, R. Robie, S. Rowan, and I. W. Martin, "Mirror coating solution for the cryogenic Einstein telescope," Phys. Rev. Lett. **122**, 231102 (2019).

46. G. D. Cole, W. Zhang, M. J. Martin, J. Ye, and M. Aspelmayer, "Tenfold reduction of Brownian noise in high-reflectivity optical coatings," Nat. Photonics **7**, 644–650 (2013).

47. P. G. Murray, I. W. Martin, K. Craig, J. Hough, S. Rowan, R. Bassiri, M. M. Fejer, J. S. Harris, B. T. Lantz, A. C. Lin, A. S. Markosyan, and R. K. Route, "Cryogenic mechanical loss of a single-crystalline GaP coating layer for precision measurement applications," Phys. Rev. D **95**, 042004 (2017).

48. G. D. Cole, W. Zhang, B. J. Bjork, D. Follman, P. Heu, C. Deutsch, L. Sonderhouse, J. Robinson, C. Franz, A. Alexandrovski, M. Notcutt, O. H. Heckl, J. Ye, and M. Aspelmeyer, "High-performance near- and mid-infrared crystalline coatings," Optica **3**, 647–656 (2016).

49. S. D. Penn, M. M. Kinley-Hanlon, I. A. O. MacMillan, P. Heu, D. Follman, C. Deutsch, G. D. Cole, and G. M. Harry, "Mechanical ringdown studies of large-area substrate-transferred GaAs/AlGaAs crystalline coatings," J. Opt. Soc. Am. B **36**, C15–C21 (2019).

50. A. V. Cumming, K. Craig, I. W. Martin, R. Bassiri, L. Cunningham, M. M. Fejer, J. S. Harris, K. Haughian, D. Heinert, B. Lantz, A. C. Lin, A. S. Markosyan, R. Nawrodt, R. Route, and S. Rowan, "Measurement of the mechanical loss of prototype GaP/AlGaP crystalline coatings for future gravitational wave detectors," Class. Quantum Grav. **32**, 035002 (2015).

51. R. Bassiri, K. Evans, K. B. Borisenko, M. M. Fejer, J. Hough, I. MacLaren, I. W. Martin, R. K. Route, and S. Rowan, "Correlations between the mechanical loss and atomic structure of amorphous TiO_2-doped Ta_2O_5 coatings," Acta Mater. **61**, 1070–1077 (2013).

52. M. Granata, E. Coillet, V. Martinez, V. Dolique, A. Amato, M. Canepa, J. Margueritat, C. Martinet, A. Mermet, C. Michel, L. Pinard, B. Sassolas, and G. Cagnoli, "Correlated evolution of structure and mechanical loss of a sputtered silica film," Phys. Rev. Mater. **2**, 053607 (2018).

53. A. Amato, S. Terreni, M. Granata, C. Michel, B. Sassolas, L. Pinard, M. Canepa, and G. Cagnoli, "What can we learn from Urbach energy of amorphous oxides thin films: experimental correlation between optical and mechanical properties," arXiv:1903.06094 (2019).

54. R. Hamdan, J. P. Trinastic, and H. P. Cheng, "Molecular dynamics study of the mechanical loss in amorphous pure and doped silica," J. Chem. Phys. **141**, 054501 (2014).

55. J. P. Trinastic, R. Hamdan, C. Billman, and H.-P. Cheng, "Molecular dynamics modeling of mechanical loss in amorphous tantala and titania-doped tantala," Phys. Rev. B **93**, 014105 (2016).

56. K. Prasai, J. Jiang, A. Mishkin, B. Shyam, S. Angelova, R. Birney, D. A. Drabold, M. Fazio, E. K. Gustafson, G. Harry, S. Hoback, J. Hough, C. Lévesque, I. MacLaren, A. Markosyan, I. W. Martin, C. S. Menoni, P. G. Murray, S. Penn, S. Reid, R. Robie, S. Rowan, F. Schiettekatte, R. Shink, A. Turner, G. Vajente, H.-P. Cheng, M. M. Fejer, A. Mehta, and R. Bassiri, "High precision detection of change in intermediate range order of amorphous zirconia-doped tantala thin films due to annealing," Phys. Rev. Lett. **123**, 045501 (2019).

57. F. Puosi, F. Fidecaro, S. Capaccioli, D. Pisignano, and D. Leporini, "In silico broadband mechanical spectroscopy of amorphous tantala," Phys. Rev. Res. **1**, 033121 (2019).